THE JOURNAL OF PHYSICAL CHEMISTRY C
A JOURNAL OF THE AMERICAN CHEMICAL SOCIETY

pubs.acs.org/JPCC

Article

Detecting Centrosymmetric Molecular Ions at an Interface with Vibrational Sum Frequency Generation Spectroscopy

Published as part of The Journal of Physical Chemistry C special issue "Vicki H. Grassian Festschrift".

Bijoya Mandal, Somaiyeh Dadashi, Koichi Kumagai, Tomonori Hirano, Tatsuya Ishiyama, Salsabil Abou-Hatab, Yunqian Zou, Spiridoula Matsika, Akihiro Morita,* and Eric Borguet*

Cite This: *J. Phys. Chem. C* 2024, 128, 21508−21517

Read Online

ACCESS | Metrics & More | Article Recommendations | Supporting Information

ABSTRACT: Under the electric dipole approximation, second-order nonlinear optical phenomena, such as vibrational sum frequency generation (vSFG) and second harmonic generation (SHG), are forbidden in centrosymmetric environments, making them surface-specific processes where the centrosymmetry is inherently broken and suitable for studying interfacial chemistry. Although the underlying theory of vSFG/SHG pertaining to centrosymmetry has been extensively studied, fundamental questions remain to be addressed. For example, what leads to the breaking of centrosymmetry in a centrosymmetric molecule at interfaces? Is the interface capable of perturbing the environment of a centrosymmetric molecule, rendering it vSFG active? At what point does the centrosymmetric molecule lose its centrosymmetry to become vSFG active? In this work, we address such basic questions by studying the vSFG response from the azido stretch of N_3^-, a centrosymmetric molecule, at the α-$Al_2O_3(0001)/H_2O$ interface. We observed the azido asymmetric stretch vSFG response at the aqueous alumina interface. There are several possible mechanisms that render this centrosymmetric molecule vSFG active, including dipole and quadrupole mechanisms. Therefore, we analyzed the possible vSFG mechanisms of the azide signal via electronic structure calculations and AIMD simulations. We show that a uniaxial electric field acting on centrosymmetric azide, whose modes are either IR or Raman active but never both, can make modes simultaneously IR and Raman active, but this turns out not to be enough to explain the sum frequency activity that we observe. The electronic structure calculations revealed that azide has sufficiently large quadrupolar susceptibility, which provides the dominant contribution in the azide vSFG response.

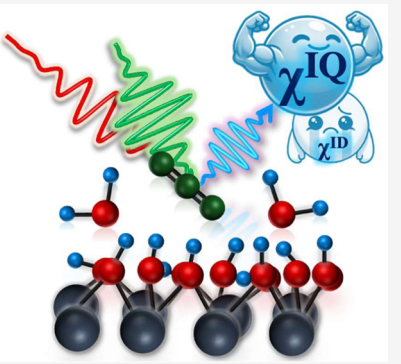

1. INTRODUCTION

1.1. Importance of Aqueous Interfaces and Mineral-Oxide/Water Interfaces. Aqueous interfaces are ubiquitous in nature and technology, making it crucial to study their behavior and properties to gain a molecular-level understanding of interfaces. Mineral oxide−water interfaces, specifically, play a significant role in mineral dissolution, soil corrosion, delta formation, heterogeneous catalysis, and microelectronics.[1−5] Hence, it is important to understand how the solvent and presence of ions affect the interfacial chemistry and microscopic properties of mineral-oxide surfaces.

1.2. Challenges to Studying Interfaces. There are challenges to studying buried interfaces using linear spectroscopic or electron-based techniques. Fourier transform infrared (FTIR) spectroscopy, a linear spectroscopy, provides information both from the bulk and the interface.[6,7] The bulk signal, typically orders of magnitude higher than the interfacial signal, obscures the interfacial response. Electron-based techniques have limitations of requiring vacuum conditions for experiments and have issues with the penetration depth. Laser-based nonlinear spectroscopic techniques, such as vibrational sum frequency generation (vSFG) and second harmonic generation (SHG), overcome many of these challenges and have widely been used to study interfaces with excellent selectivity and sensivity.[8−13]

1.3. vSFG as an Interface Specific Technique. vSFG, a second-order nonlinear optical process, is only generated from noncentrosymmetric molecules and environments, under the electric dipole approximation.[8,9] In liquids, molecules are randomly oriented and the medium is isotropic, making the bulk vSFG inactive.[11,12] Centrosymmetry is broken at any interface between two bulk media, making vSFG an inherently interface specific and surface-sensitive technique.[11,12] In a conventional vSFG experiment, an infrared (IR) beam is

Received: August 14, 2024
Revised: October 19, 2024
Accepted: October 25, 2024
Published: December 4, 2024

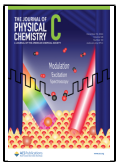

spatially and temporally overlapped with a visible (Vis) beam at an interface of interest, generating sum frequency photons at the summed frequency of the input IR and Vis frequencies.[14−16] The input IR beam frequency is chosen to be in resonance with molecular vibrations at the interface of interest.

1.4. Previous Centrosymmetric Examples. Under the electric dipole approximation, vSFG requires the interfacial molecules to be noncentrosymmetric, i.e., only vibrational modes that are both IR and Raman active provide a response. The mutual exclusion principle requires that the vibrational modes of centrosymmetric molecules are either IR active or Raman active, making them vSFG inactive. Due to the inherent surface-specific nature of the vSFG process, it is believed that centrosymmetric (i.e., nonpolar) molecules at interfaces cannot be probed by vSFG. Contrary to this belief, vSFG is actually observed at the benzene/air,[17−21] silica/fullerene,[22] and CaF_2/fullerene[22] interfaces even though benzene and fullerene are both centrosymmetric molecules. Higher vSFG intensities were observed for the A_g vibrational mode compared to the F_{1u} mode at the CaF_2/fullerene[22] vs silica/fullerene[22] interfaces depending on the interfacial surface charge and C_{60}-surface interactions.[22] The larger ratio of the A_g to F_{1u} vSFG responses at the CaF_2/fullerene interface[22] was attributed to stronger perturbation of C_{60} molecules due to the negatively charged surface of CaF_2 (ionic crystal, presence of F^- ions at the surface) than the SiO_2 surface (neutral or slightly negatively charged). It was concluded that the molecular symmetry of C_{60} films was broken at the interface, due to the chemical asymmetry of the interfacial environment, and that the higher-order quadrupole contribution to the vSFG was quite small.[22] The liquid benzene−air interface has been studied experimentally and theoretically,[18−21,23] and its vSFG response was determined to have dipole (surface) and quadrupole (bulk) contributions, indicating that vSFG cannot be solely explained within the framework of the dipole approximation and that quadrupole transitions play a crucial role.[18,20,23] Hence, there is a lack of consensus in the literature as to whether the quadrupole terms or the perturbation due to interface causes the origin of noncentrosymmetry in a centrosymmetric molecule at interfaces.[24−26]

1.5. Our Work. Though the underlying theory has been reported, unanimity regarding the origin of vSFG/SHG response from noncentrosymmetric molecules at the interface has not been reached. Is the interface capable of sufficiently perturbing the environment of a centrosymmetric molecule to render it vSFG active? Do higher-order multipole terms always contribute to vSFG? Do both of these factors act simultaneously? In this research, we address these basic questions by studying the vSFG response from the asymmetric azido stretch of N_3^-, a centrosymmetric molecule, at the α-$Al_2O_3(0001)/H_2O$ interface. The vibrational modes of N_3^- are either IR or Raman active; consequently, it is hypothesized to be vSFG inactive. However, we observed the azido asymmetric stretch peak at the aqueous alumina interface, which suggests that the interface sufficiently perturbs the centrosymmetric environment of the azide ion, making it vSFG active, thereby proving the surface specificity of the vSFG technique.

Additionally, N_3^- is an IR probe molecule whose vibrational frequency is sensitive to the local solvent environment and shifts as a function of applied electric potential or depending on solvent polarity.[27,28] The asymmetric azido stretch red-shifts in aprotic solvents (such as THF, DMSO), where H-bonding is absent, compared to H_2O and D_2O.[29] α-$Al_2O_3(0001)$ is covered with terminal hydroxyl groups that can be protonated/deprotonated depending on the bulk solution pH, resulting in the formation of localized charged sites that are heterogeneously distributed over the surface.[15,30] The shifts in the central frequency of the asymmetric stretch mode of N_3^- can, in principle, report on the interfacial localized surface potential of Al_2O_3 surfaces.

There are three possible mechanisms of vSFG from the azide ion at the alumina−water interface[31,32]

(1) χ^{ID}: dipole response originating from azide whose centrosymmetry is broken at the interface.
(2) χ^{IQ}: response from the quadrupole of azide at the interface via the interaction with the local field gradient.
(3) χ^{IQB}: direct quadrupole response from the azide.

The first term, χ^{ID}, describes the conventional dipole mechanism of SFG from noncentrosymmetric systems, whereas the latter two terms, χ^{IQ} and χ^{IQB}, are the quadrupole sources. The possibility of quadrupole mechanisms has been suggested for other molecules, including the bend mode of water[18] and C−H stretch modes of benzene.[20] We quantitatively evaluated these three terms in the present system by molecular dynamics (MD) simulation and quantum chemical calculations of susceptibilities.[33]

In our first attempt to explain the observations of sum frequency activity in the centrosymmetric molecule, we applied a static electric field to the molecule breaking its centrosymmetry to allow its vibrational modes to be both IR and Raman active. However, this approach was not sufficient to explain the sum frequency response from the azide molecule. Hence we carried out *ab initio* molecular dynamics (AIMD) calculations of azide ions located at the alumina−water interface to investigate the orientation and deformed structure of the azide ion. Then we calculated the hyperpolarizability components of azide by quantum chemical calculations. By combining the calculated hyperpolarizabilities with the information on the orientational distribution, structural deformation of azide, and Fresnel factors, we evaluated the susceptibility amplitude relevant to each of the above three mechanisms and thereby identified the dominant mechanism in the present system.

2. EXPERIMENTAL DETAILS

2.1. vSFG Experimental Setup. Details of the optical setup are provided in the literature and briefly summarized in the Supporting Information, page 2.[15,16]

2.2. Sample Preparation. The alumina sample preparation is described in the Supporting Information, page 1. The azide solutions are basic in nature (the acid HN_3 has a pK_a = 4.8), and their pH varies from 6−9 depending on their concentration. The acidic and basic H_2O solutions were made by using concentrated HCl (Sigma-Aldrich, Trace SELECT grade) and NaOH (Fluka Analytical, analytical grade), respectively.

3. THEORY AND COMPUTATION

3.1. Ab Initio Calculations. Geometry optimization and vibrational frequencies calculations were performed in the gas phase and in aqueous solution using the implicit solvation model IEFPCM at the B3LYP and MP2 level of theory with basis sets 6-311+G(d), 6-311++G(d), and 6-311++G(d,p) to resolve the ground state minimum geometry of the azide ion. Scaling factors for B3LYP[34] and MP2[35] of 0.9679 and 0.9646,

https://doi.org/10.1021/acs.jpcc.4c05318
J. Phys. Chem. C 2024, 128, 21508−21517

respectively, were used to correct for systematic errors and contributions from the inclusion of HF character to approximation of the vibrational frequencies for all basis sets. The vibrational frequencies are computed analytically using the MP2 and B3LYP methods as second derivatives of the energy, with respect to the Cartesian nuclear position of the molecule. In addition, Raman intensities are calculated by MP2 by the numerical differentiation of dipole derivatives with respect to the electric field applied. IR and Raman intensities were then computed in the gas phase and aqueous solution in the presence of an external electric field ranging from 0.005 to 0.5 V/Å, which was applied along the x, y, and z axes of the molecule (z is along the molecular axis) at the MP2/6-311++G(d,p) level of theory. All calculations were performed on Gaussian16 software.[36]

3.2. MD Calculation. AIMD simulations were performed to investigate the azide at the water/α-alumina(0001) interface. The simulations were executed using the Quickstep module of the CP2K program package.[37,38] The density functional theory calculations were carried out with the Perdew−Burke−Ernzerhof (PBE) functional[39,40] with the variant of the Grimme D3 correction for dispersion,[41] Goedecker−Teter−Hutter (GTH) pseudopotentials[42] for all constituent atoms, and a combined plane-wave (400 Ry cutoff) and the DZVP basis set. The time evolution was conducted with maintaining the temperature at T = 300 K (NVT ensemble) with the Nosé−Hoover thermostat,[43,44] and the time step was set to 0.5 fs. The three-dimensional periodic boundary conditions were adopted with the cell dimensions of $L_x \times L_y \times L_z$ = 8.24 Å × 9.52 Å × 36.80 Å, and a cell contained 136 O, 128 H, 48 Al, 3 N, and 1 Na. The initial configuration was prepared on the basis of a previous AIMD simulation work for the water/alumina interface[16] by replacing SCN with NNN and K with Na. The 1 ps equilibration run and the 6 ps production run were conducted to sample the structure and orientation of azide at the water−alumina interface.

3.3. Susceptibility Calculation. The total effective susceptibility for vSFG is given by the sum of three terms mentioned above

$$\chi^{\mathrm{eff}} = \chi^{\mathrm{ID}} + \chi^{\mathrm{IQ}} + \chi^{\mathrm{IQB}} \tag{1}$$

for either SSP or PPP polarization. The susceptibility terms relevant to the SSP, SPS, PSS, and PPP polarizations are given as follows

$$\chi^{X}_{\mathrm{SSP}} = L_y(\mathrm{SFG})L_y(\mathrm{vis})L_z(\mathrm{IR})\sin\theta(\mathrm{IR})\chi^{X}_{yyz} \quad (X = \mathrm{ID, IQ, IQB}) \tag{2}$$

$$\chi^{X}_{SPS} = L_y(SFG)L_z(vis)L_y(IR)\sin\theta(vis)\chi^{X}_{yzy} \tag{3}$$

$$\chi^{X}_{\mathrm{PSS}} = L_z(SFG)L_y(vis)L_y(IR)\sin\theta(SFG)\chi^{X}_{zyy} \tag{4}$$

$$\begin{aligned}\chi^{X}_{\mathrm{PPP}} &= -L_x(\mathrm{SFG})L_x(\mathrm{vis})L_z(\mathrm{IR})\cos\theta(\mathrm{SFG})\cos\theta(\mathrm{vis})\\ &\quad \sin\theta(\mathrm{IR})\chi^{X}_{xxz}\\ &\quad -L_x(\mathrm{SFG})L_z(\mathrm{vis})L_x(\mathrm{IR})\cos\theta(\mathrm{SFG})\sin\theta(\mathrm{vis})\cos\theta(\mathrm{IR})\chi^{X}_{xzx}\\ &\quad +L_z(\mathrm{SFG})L_x(\mathrm{vis})L_x(\mathrm{IR})\sin\theta(\mathrm{SFG})\cos\theta(\mathrm{vis})\cos\theta(\mathrm{IR})\chi^{X}_{zxx}\\ &\quad +L_z(\mathrm{SFG})L_z(\mathrm{vis})L_z(\mathrm{IR})\sin\theta(\mathrm{SFG})\sin\theta(\mathrm{vis})\sin\theta(\mathrm{IR})\chi^{X}_{zzz}\end{aligned} \tag{5}$$

where the superscript X denotes either ID, IQ or IQB. L denotes the Fresnel factors, and θ(vis), θ(IR), and θ(SFG) are the incident/radiation angles of the visible, infrared (IR), and sum frequency photons, respectively. These angles and the Fresnel factors were determined from the experimental conditions at the α-alumina/water interface, as shown in the Supporting Information, page 15.

χ^{X}_{pqr} ($p,q,r = x,y$ or z) on the right-hand side of eqs 2 and 5 are the susceptibility tensor components in the space-fixed coordinates, and are represented as follows

$$\chi^{\mathrm{ID}}_{pqr} = f_p(\mathrm{SFG})f_q(\mathrm{vis})f_r(\mathrm{IR})\rho\langle\alpha^{D0}_{pqr,\mathrm{space}}\rangle \tag{6}$$

$$\begin{aligned}\chi^{\mathrm{IQ}}_{pqr} = \sum_{s}^{x-z}\Bigg\{ & f_p(\mathrm{SFG})\frac{\partial f_q(\mathrm{vis})}{\partial s}f_r(\mathrm{IR})\rho\langle\alpha^{D1}_{pqrs,\mathrm{space}}\rangle\\ & + f_p(\mathrm{SFG})f_q(\mathrm{vis})\frac{\partial f_r(\mathrm{IR})}{\partial s}\rho\langle\alpha^{D2}_{pqrs,\mathrm{space}}\rangle\\ & + \frac{\partial f_p(\mathrm{SFG})}{\partial s}f_q(\mathrm{vis})f_r(\mathrm{IR})\rho\langle\alpha^{\mathrm{Q}}_{pqrs,\mathrm{space}}\rangle\Bigg\}\end{aligned} \tag{7}$$

$$\begin{aligned}\chi^{\mathrm{IQB}}_{pqr} = & -if_p(\mathrm{SFG})f_q(\mathrm{vis})f_r(\mathrm{IR})\frac{n(\mathrm{alumina})\Omega\cos\theta(\mathrm{SFG})}{c}\\ & \rho\langle\alpha^{\mathrm{Q}}_{pqrz,\mathrm{space}}\rangle\end{aligned} \tag{8}$$

where ρ and $\langle\alpha^{Y}_{pqr,\mathrm{space}}\rangle$ (Y = D0, D1, D2, Q) are the number density and hyperpolarizability components of the azide ion, respectively. f and $\frac{\partial f}{\partial s}$ denote the local field correction factor and its gradient, respectively. n (alumina), Ω, c in eq 8 are the refractive index of the alumina substrate, the vSFG frequency, and the speed of light in vacuum, respectively.

The hyperpolarizability components in the space-fixed coordinates were calculated from those in the molecule-fixed coordinates by the rotation matrix D

$$\begin{aligned}\langle\alpha^{D0}_{pqr,\mathrm{space}}\rangle &= \Big\langle\sum_{p'q'r'} D_{pp'}D_{qq'}D_{rr'}\alpha^{D0}_{p'q'r',\mathrm{mol}}\Big\rangle\\ \langle\alpha^{Y}_{pqrs,\mathrm{space}}\rangle &= \Big\langle\sum_{p'q'r's'} D_{pp'}D_{qq'}D_{rr'}D_{ss'}\alpha^{Y}_{p'q'r's',\mathrm{mol}}\Big\rangle\\ & \quad (Y = \mathrm{D1, D2, Q})\end{aligned} \tag{9}$$

where p', q', r', s' are the suffixes $x \sim z$ in the molecule-fixed coordinates, and $\langle\,\rangle$ denotes the statistical average. The rotation matrix D and its distribution were obtained from the MD simulation.

The molecular hyperpolarizabilities in the molecule-fixed coordinates $\alpha^{Y}_{p'q'r',\mathrm{mol}}$ (Y = D0, D1, D2, Q) in eq 9 were calculated using Qsac,[33] as detailed in the Supporting Information, page 10. To briefly summarize the procedure, we obtained $\alpha^{Y}_{p'q'r',\mathrm{mol}}$ by the calculations of dipole, dipole polarizability, quadrupole, and quadrupolar polarizabilities of azide and their transition properties (derivatives with respect to the normal mode coordinate) by B3LYP and aug-cc-pVTZ. Those properties were calculated for the azide of deformed geometries and under external fields, since the contribution of noncentrosymmetric molecules is essential in the dipole mechanism of vSFG, χ^{ID} in eq 6. The calculation of eq 9 took into account both the molecular orientation and the deformation that were sampled from the MD simulation.

https://doi.org/10.1021/acs.jpcc.4c05318
J. Phys. Chem. C 2024, 128, 21508−21517

4. RESULTS AND DISCUSSION

4.1. Experimental Spectra. *4.1.1. vSFG Spectra of N_3^- at $Al_2O_3(0001)/H_2O$ Interface. 4.1.1.1. Effect of Azide Concentration.* To probe the azide asymmetric stretch and investigate the adsorption behavior of azide ions at the $Al_2O_3(0001)/H_2O$ interface, we recorded the vSFG spectra of N_3^- at different NaN_3 concentrations (0.01−2 M) revealing a feature in the 1900−2150 cm^{-1} frequency region (Figure 1) which was assigned to the asymmetric stretch mode. The water combination band (bend + libration) ∼2100 cm^{-1} is a broad peak with fwhm ∼200 cm^{-1}[45,46] was ruled out as the origin of the feature because the vSFG response in the 1900−2150 cm^{-1} region was low (Figure 1, light blue curve) compared to vSFG response from $Al_2O_3(0001)/H_2O$ (with azide ions) (Figure 1). Initially, there is an enhancement in the vSFG signal with increasing azide molarity (0.01−0.5 M). At high azide concentration (1−2 M), we observed a decrease in the vSFG intensity at the lower frequency region (∼2000 cm^{-1}) and increase in the vSFG signal at higher frequency region (∼2100 cm^{-1}).

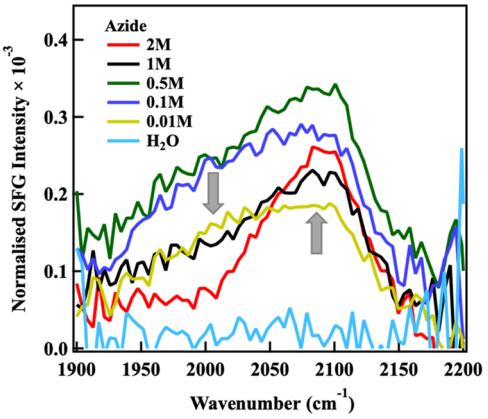

Figure 1. vSFG spectra at the $Al_2O_3(0001)/H_2O$ interface with different concentrations of N_3^- ions (0.01 M−2 M) in the azido stretching region measured in the PPP (polarizations of the vSFG, visible, and IR photons listed in the order of decreasing photon energy) polarization combination.

The vSFG results are similar to the work by Philpott *et al.* who studied the *in situ* infrared vibrational spectroscopy of specifically adsorbed azide on a silver electrode and observed a peak and a shoulder for N_3^- asymmetric stretch.[28] The main peak at 2050 cm^{-1} (not dependent on the applied potential of the electrode) corresponded to bulk N_3^- asymmetric stretch and the shoulder at ∼2083 cm^{-1} (dependent on the applied potential of the electrode) was attributed to the N_3^- asymmetric stretch that probes the electric field at the electrode surface.[28]

The alumina surface is covered with hydroxyl groups that can be neutral, protonated, or deprotonated based on the bulk pH of the solution being used.[16] Previous reports of SCN^- at the $Al_2O_3(0001)/H_2O$ surface revealed that the anion probed the different localized sites on alumina and measured their respective electrostatic potentials.[16] We wanted to expand the library of probe molecules using N_3^-, a Stark active molecule, to measure the electrostatic potentials at the heterogeneously

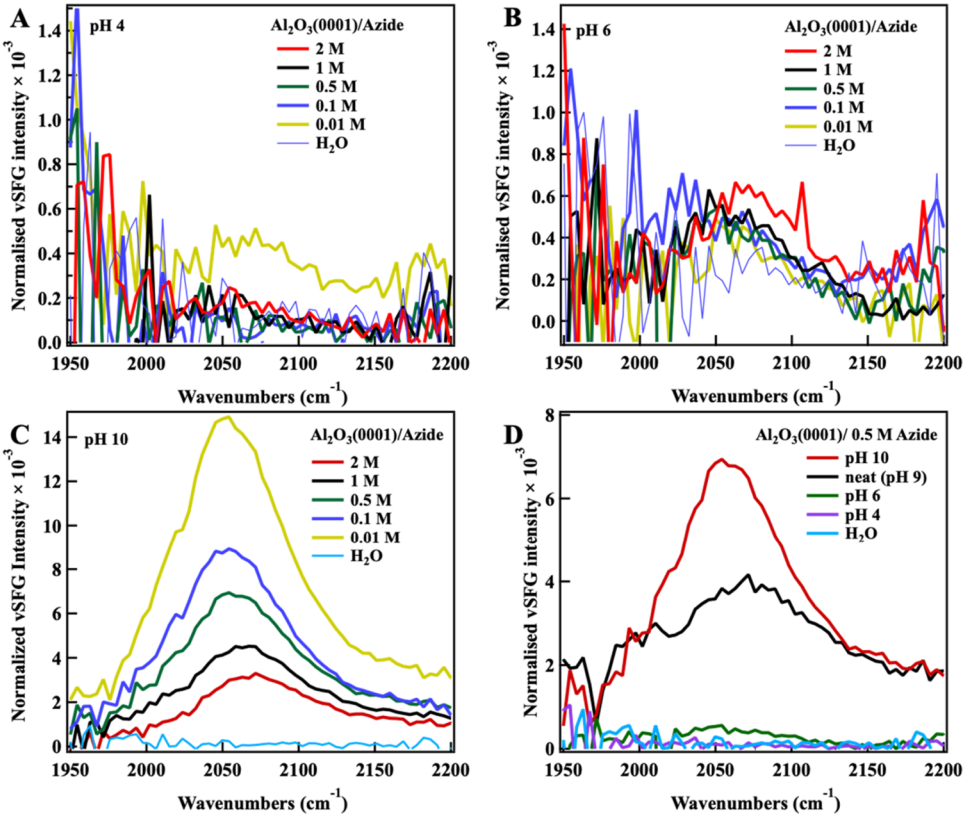

Figure 2. Concentration and pH-dependent vSFG spectra at the $Al_2O_3(0001)/H_2O$ interface with azide ions (0.01 M−2 M) at pH 4 (A), pH 6 (B), pH 10 (C), and comparison of vSFG spectra of 0.5 M azide solution at the $Al_2O_3(0001)/H_2O$ interface at pH 4, 6, 9 (neat azide solution), and 10 (D) using the PPP polarization combination (P-polarized vSFG, Vis, and IR).

https://doi.org/10.1021/acs.jpcc.4c05318
J. Phys. Chem. C 2024, 128, 21508−21517

distributed localized sites on $Al_2O_3(0001)$ as well as test the reliability and robustness of the site specific nature of the technique. This led us to perform vSFG experiments at the $Al_2O_3(0001)/H_2O$ interface with azide ions at bulk solution pH 4, 6, and 10, corresponding to a positively charged, neutral, and negatively charged surface. We observed that the neat azide solutions with different concentrations had pH in the range 7−9 (Supporting Information, Table S1).

4.1.1.2. Effect of pH. The neat azide solutions with different concentrations (0.0001−2 M) had bulk pH ranging from pH 7 to pH 9 (Supporting Information, Table S1) that resulted in pH-dependent charging of the Al_2O_3 surface due to protonation/deprotonation of terminal hydroxyl groups.[14,16,47] Thus, changing the concentration of the azide meant varying not just one parameter but two parameters (azide concentration and alumina surface charge) simultaneously. Hence, next we performed experiments by having a constant pH for all the azide solutions. The commonly reported PZC of Al_2O_3 is in the range pH (6−8) where the surface is charge neutral.[48−50] At pH 4 and 6, the vSFG response from the azide solutions was low and a clear peak was not observed (Figure 2A,B), whereas at pH 10, a distinct peak corresponding to the azide asymmetric stretch was observed (Figure 2 C). The possible reason for not observing the N_3^- asymmetric stretch peak at acidic pH is the absence of azide ions and formation of HN_3 (pK_a = 4.8), which shows up at a higher frequency ∼2150 cm^{-1}, at the edge of our probe window.[51,52] The concentration of HN_3 is 4 times higher than that of N_3^- at pH 4 (detailed calculation shown in Supporting Information page 18).

The concentration dependent vSFG spectra at pH 10 have only 1 peak (Figure 2C). The highest vSFG intensity occurs for the 0.01 M azide solution. Then, the vSFG signal decreases and blue shifts with increasing azide concentration (Figure 2C). This observation differs from the previous concentration dependent vSFG spectra reported (Figure 1) where the pH of the solutions was not kept constant but rather shifted to more basic values with a higher SCN^- concentration.

4.1.1.3. Effect of Different Polarization Combinations. To probe the different elements of the $\chi^{(2)}$ tensor, vSFG spectra were recorded with different polarization combinations (eqs 2−5). No response, that could be associated with the azido stretching vibrations, was observed in the PSP, SSP, and SPP polarization combination vSFG spectra (Figure S2) at the $Al_2O_3(0001)/H_2O$ interface over the concentration range of N_3^- ions (0.01 M−2 M) explored. This suggests that the azide molecules are mostly adsorbed perpendicular to the surface.

4.1.1.4. Ab Initio Calculations. The azide ion in the bulk solvent should be vSFG inactive, as it is a centrosymmetric molecule (its vibrational modes are either IR or Raman active under the mutual exclusion principle) in an isotropic environment (bulk water). The vibrational modes of N_3^- in aqueous solutions are the 2-fold degenerate bending mode (640 cm^{-1}, IR active), the symmetric stretch mode (1340 cm^{-1}, Raman active), and asymmetric stretch mode (2050 cm^{-1}, IR active).[27,28] The vSFG spectra show that the interaction of the azide ions with the oxide surface and the presence of an interface (oxide/water) have the potential to break the symmetry of the molecule and introduce IR and/or Raman activities in the vibrational modes where it was initially absent.

To understand the effect of applied external electric fields on the azide ions, first, the vibrational frequency of the azide asymmetric stretch was benchmarked with different levels of theory and basis sets (Table 1) to identify a reliable method that can predict its nature without the presence of an external electric field. Experimentally, the asymmetric stretch of azide in the gas phase is at ∼1986 cm^{-1} and in aqueous solution it blue shifts to 2048 cm^{-1} due to H-bonding with H_2O.[27,51] The B3LYP hybrid function of the DFT method does not give an accurate qualitative description of the solvatochromic shift (shift in the vibrational frequency between the gas and aqueous phases), showing a red-shift rather than a blue-shift in an aqueous solution compared to the gas phase. The *ab initio* MP2 method was found to accurately describe the direction of the solvatochromic shift but still underestimates its magnitude by 19 cm^{-1}. The size of the basis set was found to have no effect on the vibrational frequency when computed both in the gas phase and in an aqueous solution. As a result, we continue to investigate the effect of applied external electric fields on the IR and Raman intensity of azide ions at the MP2/6-311++G(d,p) level of theory.

Table 1. Vibrational Frequency of the Symmetric Stretch Mode of the Azide Ion (cm^{-1})

method/basis set	gas phase	aqueous solution	solvatochromic shift
B3LYP/6-311+G(d)	1996	1965	−31
B3LYP/6-311++G(d)	1996	1965	−31
B3LYP/6-311++G(d,p)	1996	1965	−31
MP2/6-311++G(d,p)	2078	2121	43
MP2/6-311++G(d)	2078	2121	43
MP2/6-311+G(d)	2078	2121	43
exp	1986	2048	62

Considering that the alumina surface has heterogeneously distributed, localized charged sites generating an interfacial electrostatic potential that causes shift in the vibrational frequency of IR probe molecules (such as SCN^-,[16] and N_3^-,), we wanted to investigate the effect of a static electric field on the N_3^- ions in solvent using MP2 calculations. The calculation of the vibrational modes of N_3^- in the gas phase predicts two degenerate bending modes (IR active, Raman inactive), symmetric stretch (Raman active, IR inactive), and asymmetric stretch (IR active, Raman inactive) (Figure 3A). The IR intensity of the asymmetric stretch of the azide ion in an aqueous solution (using implicit solvation model IEFPCM) grows with an increasing external electric field (0.005−0.5 V/angstroms) applied along the x, y, and z axes (Figure 3C). There is no Raman activity in the azide asymmetric stretch when the electric field is applied along the x and y directions (perpendicular to the molecular plane) (Figure 3B). However, Raman activity is observed and enhanced as the external electric field is applied in the z direction (molecular plane) (Figure 3B), the molecular axis that corresponds to the maximum electron density and, hence, maximum induced polarizability anisotropy with the application of the electric field. The MP2 results show that an external electric field of the order 0.005 to 0.5 V/Å, mimics the range of observed electrostatic potentials and double layers at interfaces.[22,53−55] This introduces Raman activity to the asymmetric mode that was initially Raman forbidden, leading to the vibrational mode being vSFG active. Whether this breaking of the centrosymmetry is sufficient to explain the experimental observations is addressed in the AIMD calculations discussed below.

https://doi.org/10.1021/acs.jpcc.4c05318
J. Phys. Chem. C 2024, 128, 21508−21517

Vibrational modes		IR Intensity (Gas phase)	Raman Activity (Gas phase)
A 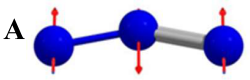	Bending	7	0
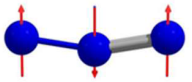	Bending	7	0
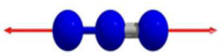	Symmetric stretch	0	37
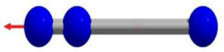	Asymmetric stretch	1242	0

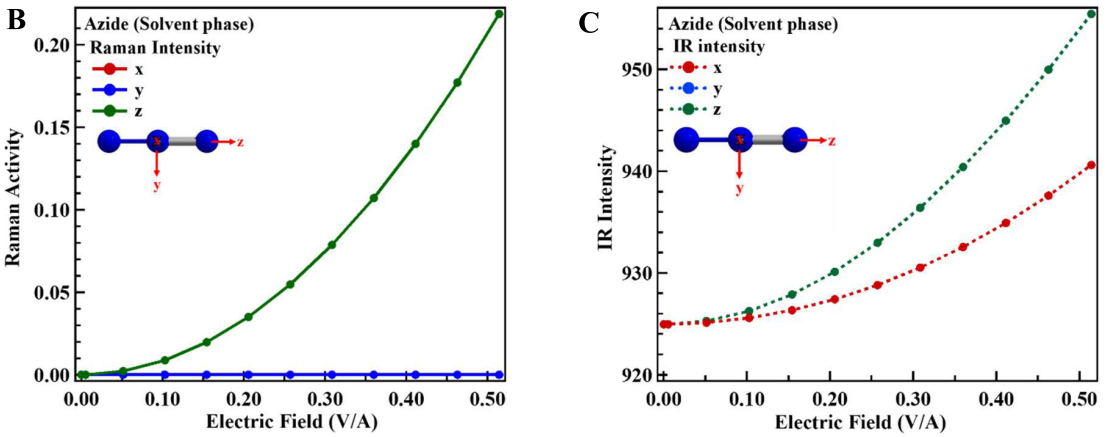

Figure 3. MP2/6-311++G(d,p) calculations of the N_3^- ion showing the four different vibrational modes (A), effect of an external electric field applied in the x (red curve), y (blue curve), and z (green curve) direction on the azide asymmetric stretch Raman intensity (B) and on the IR intensity (C). The z direction is along the molecular axis. The blue curve is on top of the red curve and hence not visible in plot B. Similarly, the red curve is on top of the blue curve in plot C and not observed. The effect of the external electric field along the x and y directions is the same.

4.1.1.5. MD Results. The MD simulations presented here evaluate the surface environment that the azide experiences at the α-alumina (0001)/water interface, as illustrated in Figure 4(a). In this figure, r_1 (r_2) represents the distance between N1 and N2 (N2 and N3), where the nitrogen sites N1, N2 and N3 are labeled in order of increasing distance from the alumina surface. Figure 4(b) shows the intramolecular configuration of azide, where the asymmetric deformation is defined with $\Delta r = r_1 - r_2$.

The MD simulation results allow for the probability distributions about the azide configuration at the alumina surface to be determined. Figure 5(a) shows that there is a broad distribution of tilt angles and the perpendicular orientation ($\cos\theta \sim 1$) is rather minor. The cosine of $N_1-N_2-N_3$ is close to -1 in Figure 5(b), indicating a nearly linear molecular geometry and the bend deformation is negligibly small. In Figure 5(c), the distribution of asymmetric deformation, $\Delta r = r_1-r_2$, tends to be positive and the mean Δr is 0.019 Å. The positive deformation $\Delta r > 0$ is induced when the N_1 site is attached to a hydrogen of the alumina surface and slightly assumes the character of electronic

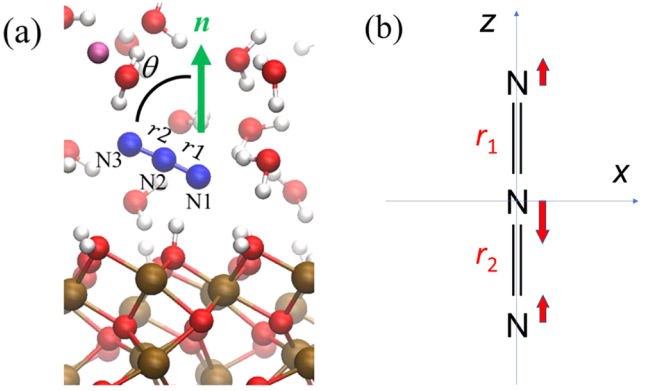

Figure 4. (a) Snapshot of AIMD simulation for azide at the α-alumina(0001)−water interface. The nitrogen sites were labeled with N1, N2, and N3 in the increasing order of distance from the alumina surface. θ is the tilt angle (0−90°) of the N1−N3 vector from the surface normal $\boldsymbol{n}$. (b) Azide ion and its asymmetric stretching mode in the molecule-fixed coordinates.

https://doi.org/10.1021/acs.jpcc.4c05318
J. Phys. Chem. C 2024, 128, 21508−21517

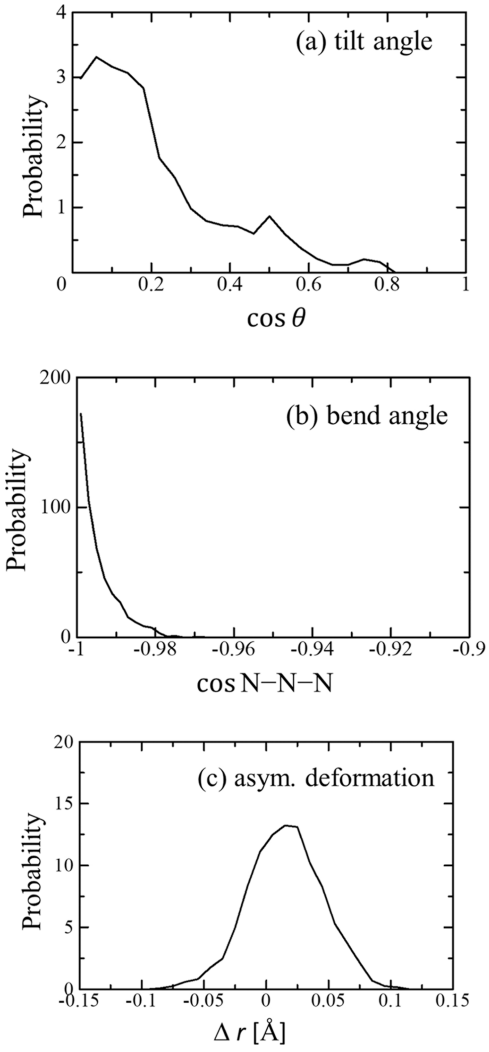

Figure 5. MD results of probability distributions about azide configuration at alumina surface, (a) cos θ, (b) cosine of N_1–N_2–N_3 bend angle, and (c) $\Delta r = r_1 - r_2$.

structure $[N_1^- \leftarrow N_2 \equiv N_3]$. The charge distribution and electronic structure of azide is sensitive to the antisymmetric deformation.[56] The valence-bond structure of azide at the equilibrium conformation consists of the main resonance component $[N_1^- = N_2^+ = N_3^-]$ and two equivalent minor components $[N_1^- \leftarrow N_2 \equiv N_3]$ and $[N_1^- \equiv N_2 \rightarrow N_3^-]$. The asymmetric deformation breaks the centrosymmetry and enhances the character of minor components. The MD results of the orientation and deformation are used to estimate various vSFG mechanisms below.

4.1.1.6. Estimated Susceptibility Components. By combining the above MD results of orientation and deformed conformation, quantum chemical calculations of the transition properties, and the Fresnel factors, we evaluate the susceptibility components χ^{ID}, χ^{IQ}, and χ^{IQB} of azide ion in eqs 6–8, respectively. To compare the relative amplitudes of these terms, we assumed $\rho = 1$ and $f = 1$ in these equations, since these factors are common. $\partial f/\partial z$ was estimated to be ~1 nm^{-1} from the density profile of the interfacial water layer.[57] The gradient of the optical local field is rather short ranged, as its screening profile is correlated with the density profile of water.[58] The present estimate is sufficient to evaluate the magnitude of χ^{IQ}, although the quantitative optical screening profile depends on the conditions of the interface. The relative magnitudes of these terms were represented with the integrated amplitudes $S[\chi^X]$ (X = ID, IQ, IQB) over the frequency range of the asymmetric stretching band

$$S[\chi^X] = \int_{\text{band}} \chi^X(\omega) d\omega \qquad (X = \text{ID, IQ, IQB}) \tag{10}$$

$S[\chi^X]$ (X = ID, IQ, IQB) were derived for SSP and PPP polarizations (see eqs 2 and 5) and is summarized in Table 2. Table 2 is the main result of the present calculations from which we derive the following two conclusions.

Comparing the PPP and SSP polarizations, the PPP amplitude is several times stronger. This was confirmed by the experimental observations (Figure S2).

Comparing the three mechanisms χ^{IQ}, χ^{ID}, and χ^{IQB}, one finds that the vSFG signal from azide is mainly attributed to the χ^{IQ} term, indicating vSFG radiation from the quadrupole interaction with the local field gradient at the interface. The χ^{ID} term, which refers to the dipole response from distorted noncentrosymmetric azide at the interface, is relatively small in the present system, and the direct quadrupole χ^{IQB} term is almost negligible.

The main purpose of the present calculations is to compare the amplitudes associated with various vSFG mechanisms on the same footing as discussed above. To illustrate their influences on the spectra, we can expand the above discussion and roughly estimate the spectral lineshapes. Here we assumed a single complex Lorentz function for the IR frequency with the center $\omega_a = 2100$ cm^{-1} and the width $\Gamma = 70$ cm^{-1} and simulated the χ^X lineshapes of various components (X = ID, IQ, IQD) in the PPP polarization in Figure 6 (cf. Supporting Information, page 16). We notice that the amplitude of χ^{IQ} is dominant as argued above in Table 2, and the lineshapes of those χ^X (X = ID, IQ, IQB) components are distorted from a pure Lorentzian due to the complex Fresnel factors. The simulated intensity spectra $|\chi^{ID} + \chi^{IQ} + \chi^{IQB}|^2$ for PPP and SSP polarizations are shown in Figure 7, where nonresonant background is assumed to be zero.

5. CONCLUSIONS

The vSFG spectra recorded at the $Al_2O_3(0001)/H_2O$ interface as a function of bulk pH and azide concentration revealed that N_3^-, a centrosymmetric molecular anion, induces a nonlinear

Table 2. Integrated Amplitudes of χ^X (X = ID, IQ, and IQB) in PPP and SSP Polarizations[a]

	$S[\chi^{ID}]$	$S[\chi^{IQ}]$	$S[\chi^{IQB}]$
(a) PPP	$5.5 \times 10^{-3} - 4.8 \times 10^{-3}\, i$	$-1.1 \times 10^{-1} + 9.4 \times 10^{-2}\, i$	$4.5 \times 10^{-4} - 3.9 \times 10^{-4}\, i$
	(1.0)	(19)	(0.082)
(b) SSP	$-3.0 \times 10^{-3} + 7.6 \times 10^{-4}\, i$	$-6.1 \times 10^{-2} + 1.5 \times 10^{-2}\, i$	$8.1 \times 10^{-4} - 2.1 \times 10^{-4}\, i$
	(1.0)	(20)	(0.27)

[a]Unit: Atomic Units. The Values in Parentheses Are the Absolute Ratio $|S[\chi^X]/S[\chi^{ID}]|$.

https://doi.org/10.1021/acs.jpcc.4c05318
J. Phys. Chem. C 2024, 128, 21508–21517

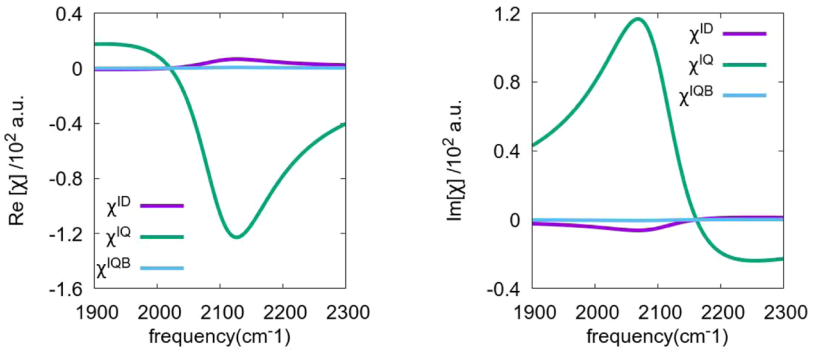

Figure 6. Estimated (left) Re[χ^X] and (right) Im[χ^X] spectra for PPP polarization.

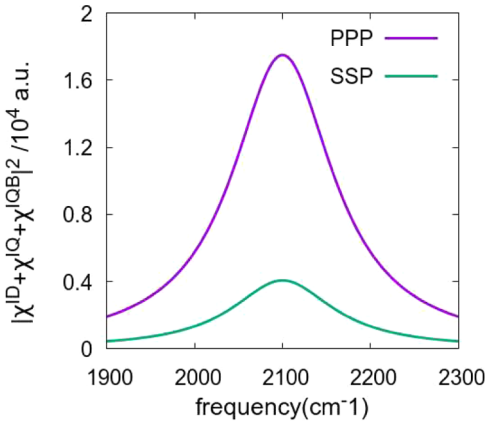

Figure 7. Calculated intensity spectra of $|\chi^{ID} + \chi^{IQ} + \chi^{IQB}|^2$ for PPP and SSP polarizations, with an assumption of no nonresonant background.

optical response. The pH-dependent experiments concluded that a vSFG signal was generated only at basic pH (pH > 7), as in acidic pH, the azide ions were converted to HN_3 shifting the vibrational frequency by at least a 100 cm^{-1} and outside our probing window. MP2 calculations revealed that application of an external electric field lifts the centrosymmetry of the azide ion, introducing some Raman activity to the IR active mode (asymmetry azide stretch), thereby making the ion vSFG active.

We also performed AIMD and quantum chemical calculations of azide and evaluated the relative contributions of the three distinct vSFG mechanisms (χ^{ID}, χ^{IQ} and χ^{IQB}) on the same footing. Comparing the three mechanisms, we found that χ^{IQ} has the major contribution in the present system of azide at the alumina surface, which indicates the dipole radiation originating from the quadrupole coupled to the field gradient at the interface. The dipole mechanism with broken symmetry χ^{ID} is rather minor, and the quadrupole radiation χ^{IQB} is almost negligible. The comparison of χ^{ID} and χ^{IQ} requires estimates of the extent of broken centrosymmetry and the optical field gradient, besides quantum chemical calculations of dipolar and quadrupolar molecular hyperpolarizabilities. This work implies that the extent of broken centrosymmetry of the azide is not large enough at the alumina surface to make χ^{ID} dominate the vSFG signal. The azide ion has intrinsically very strong quadrupole character of $N_1^-{=}N_2^+{=}N_3^-$, and accordingly large quadrupole susceptibility. We also note that the relative importance of dipole and quadrupole terms may depend on the systems, and further investigation is desirable for other centrosymmetric molecules.

■ ASSOCIATED CONTENT

Supporting Information

The Supporting Information is available free of charge at https://pubs.acs.org/doi/10.1021/acs.jpcc.4c05318.

Additional sample preparation and optical setup details, vSFG spectroscopy/data normalization, comparison of vSFG spectra of $Al_2O_3(0001)/H_2O$ in the azide stretching region with and without azide ions, effect of different polarization combinations, comparison of vSFG spectra of $Al_2O_3(0001)/H_2O$ in the azide stretching region after each azide concentration experiment, comparison of 0.1 and 2 M NaCl solution vSFG spectra in the azide stretching region, pH of different concentration of azide solutions, vSFG spectra of $Al_2O_3(0001)/H_2O$ interface with azide ions in the OH stretch region, molecular hyperpolarizabilities, effect of deformation of azide, Fresnel factors, lineshape simulation, and calculation of the concentration of HN_3 molecules in a NaN_3 solution at pH 4 (PDF)

■ AUTHOR INFORMATION

Corresponding Authors

Akihiro Morita − *Department of Chemistry, Graduate School of Science, Tohoku University, Sendai 980-8578, Japan;* orcid.org/0000-0002-2104-0605; Email: morita@tohoku.ac.jp

Eric Borguet − *Department of Chemistry, Temple University, Philadelphia, Pennsylvania 19122, United States;* orcid.org/0000-0003-0593-952X; Email: eborguet@temple.edu

Authors

Bijoya Mandal − *Department of Chemistry, Temple University, Philadelphia, Pennsylvania 19122, United States;* orcid.org/0009-0002-2059-622X

Somaiyeh Dadashi − *Department of Chemistry, Temple University, Philadelphia, Pennsylvania 19122, United States;* orcid.org/0009-0003-3249-3428

Koichi Kumagai − *Department of Chemistry, Graduate School of Science, Tohoku University, Sendai 980-8578, Japan*

Tomonori Hirano − *Department of Chemistry, Graduate School of Science, Tohoku University, Sendai 980-8578, Japan;* orcid.org/0000-0001-9772-4555

Tatsuya Ishiyama − *Department of Applied Chemistry, Graduate School of Science and Engineering, University of*

Toyama, Toyama 930-8555, Japan; orcid.org/0000-0003-2388-7727

Salsabil Abou-Hatab − *Department of Chemistry, Temple University, Philadelphia, Pennsylvania 19122, United States*

Yunqian Zou − *Department of Chemistry, Temple University, Philadelphia, Pennsylvania 19122, United States*

Spiridoula Matsika − *Department of Chemistry, Temple University, Philadelphia, Pennsylvania 19122, United States;* orcid.org/0000-0003-2773-3979

Complete contact information is available at: https://pubs.acs.org/10.1021/acs.jpcc.4c05318

Notes

The authors declare no competing financial interest.

■ ACKNOWLEDGMENTS

The authors gratefully acknowledge the support of the NSF (CHE 2102557) for the experimental work. A part of the MD calculations was performed using the supercomputers at the Research Center for Computational Science, Okazaki, Japan. This work was supported by the Grants-in-Aid (Nos. 20H00368, 21H01878) by the Japan Society for the Promotion of Science (JSPS). We are grateful to Dr. Mark DelloStritto for providing the initial configurations for the AIMD simulations. Dr. Spiridoula Matsika and Dr. Salsabil Abou-Hatab were supported by NSF (CHE-2303111).

■ REFERENCES

(1) Crundwell, F. K. On the Mechanism of the Dissolution of Quartz and Silica in Aqueous Solutions. *ACS Omega* **2017**, *2* (3), 1116−1127.

(2) Dove, P. M. The dissolution kinetics of quartz in sodium chloride solutions at 25 degrees to 300 degrees C. *Am. J. Sci.* **1994**, *294*, 665.

(3) Méndez, F. J.; Solano, R.; Villasana, Y.; Guerra, J.; Curbelo, S.; Inojosa, M.; Olivera-Fuentes, C.; Brito, J. L. Selective hydrogenation of 1,3-butadiene in presence of 1-butene under liquid phase conditions with NiPd/Al_2O_3 catalysts. *Appl. Petrochem. Res.* **2016**, *6* (4), 379−387.

(4) Knözinger, H.; Ratnasamy, P. Catalytic Aluminas: Surface Models and Characterization of Surface Sites. *Catal. Rev.* **1978**, *17* (1), 31−70.

(5) Korhonen, H.; Syväluoto, A.; Leskinen, J. T. T.; Lappalainen, R. Optically transparent and durable Al_2O_3 coatings for harsh environments by ultra short pulsed laser deposition. *Optics Laser Technol.* **2018**, *98*, 373−384.

(6) Mohamed, M. A.; Jaafar, J.; Ismail, A. F.; Othman, M. H. D.; Rahman, M. A. Chapter 1 - Fourier Transform Infrared (FTIR) Spectroscopy. *Membrane Characterization* **2017**, 3−29.

(7) Scheuing, D. R. Fourier Transform Infrared Spectroscopy in Colloid and Interface Science. *Fourier Transform Infrared Spectroscopy Colloid Interface Science* **1990**, *447* (447), 1−21.

(8) Shen, Y. R. Surface properties probed by second-harmonic and sum-frequency generation. *Nature* **1989**, *337* (6207), 519−525.

(9) Shen, Y. R.; Ostroverkhov, V. Sum-Frequency Vibrational Spectroscopy on Water Interfaces: Polar Orientation of Water Molecules at Interfaces. *Chem. Rev.* **2006**, *106* (4), 1140−1154.

(10) Shen, Y. R. Phase-Sensitive Sum-Frequency Spectroscopy. *Annu. Rev. Phys. Chem.* **2013**, *64* (1), 129−150.

(11) Vidal, F.; Tadjeddine, A. Sum-frequency generation spectroscopy of interfaces. *Rep. Prog. Phys.* **2005**, *68* (5), 1095−1127.

(12) Lambert, A. G.; Davies, P. B.; Neivandt, D. J. Implementing the Theory of Sum Frequency Generation Vibrational Spectroscopy: A Tutorial Review. *Appl. Spectrosc. Rev.* **2005**, *40* (2), 103−145.

(13) Piontek, S. M.; Borguet, E. Vibrational spectroscopy of geochemical interfaces. *Surf. Sci. Rep.* **2023**, *78* (4), No. 100606.

(14) Tuladhar, A.; Piontek, S. M.; Borguet, E. Insights on Interfacial Structure, Dynamics, and Proton Transfer from Ultrafast Vibrational Sum Frequency Generation Spectroscopy of the Alumina(0001)/Water Interface. *J. Phys. Chem. C* **2017**, *121* (9), 5168−5177.

(15) Piontek, S. M.; Tuladhar, A.; Marshall, T.; Borguet, E. Monovalent and Divalent Cations at the α-Al_2O_3(0001)/Water Interface: How Cation Identity Affects Interfacial Ordering and Vibrational Dynamics. *J. Phys. Chem. C* **2019**, *123* (30), 18315−18324.

(16) Piontek, S. M.; DelloStritto, M.; Mandal, B.; Marshall, T.; Klein, M. L.; Borguet, E. Probing Heterogeneous Charge Distributions at the α-Al_2O_3(0001)/H_2O Interface. *J. Am. Chem. Soc.* **2020**, *142* (28), 12096−12105.

(17) Hommel, E. L.; Allen, H. C. The air−liquid interface of benzene, toluene, m-xylene, and mesitylene: a sum frequency, Raman, and infrared spectroscopic study. *Analyst* **2003**, *128* (6), 750−755.

(18) Kawaguchi, T.; Shiratori, K.; Henmi, Y.; Ishiyama, T.; Morita, A. Mechanisms of Sum Frequency Generation from Liquid Benzene: Symmetry Breaking at Interface and Bulk Contribution. *J. Phys. Chem. C* **2012**, *116* (24), 13169−13182.

(19) Yamaguchi, S.; Shiratori, K.; Morita, A.; Tahara, T. Electric quadrupole contribution to the nonresonant background of sum frequency generation at air/liquid interfaces. *J. Chem. Phys.* **2011**, *134* (18), No. 184705.

(20) Matsuzaki, K.; Nihonyanagi, S.; Yamaguchi, S.; Nagata, T.; Tahara, T. Vibrational Sum Frequency Generation by the Quadrupolar Mechanism at the Nonpolar Benzene/Air Interface. *J. Phys. Chem. Lett.* **2013**, *4* (10), 1654−1658.

(21) Matsuzaki, K.; Nihonyanagi, S.; Yamaguchi, S.; Nagata, T.; Tahara, T. Quadrupolar mechanism for vibrational sum frequency generation at air/liquid interfaces: Theory and experiment. *J. Chem. Phys.* **2019**, *151* (6), No. 064701.

(22) Sohrabpour, Z.; Kearns, P. M.; Massari, A. M. Vibrational Sum Frequency Generation Spectroscopy of Fullerene at Dielectric Interfaces. *J. Phys. Chem. C* **2016**, *120* (3), 1666−1672.

(23) Sun, S.; Tian, C.; Shen, Y. R. Surface sum-frequency vibrational spectroscopy of nonpolar media. *Proc. Natl. Acad. Sci. U. S. A.* **2015**, *112* (19), 5883−5887.

(24) Hirano, T.; Kumagai, K.; Ishiyama, T.; Morita, A. Comment on ″Sum-frequency vibrational spectroscopy of centrosymmetric molecule at interfaces″. *J. Chem. Phys.* **2024**, *160* (10), No. 107101.

(25) Zheng, R. H.; Wei, W. M.; Zhang, S. C. Sum-frequency vibrational spectroscopy of centrosymmetric molecule at interfaces. *J. Chem. Phys.* **2023**, *158* (7), No. 074701.

(26) Zheng, R. H.; Wei, W. M.; Zhang, S. C. Response to ″Comment on 'Sum-frequency vibrational spectroscopy of centrosymmetric molecule at interfaces'″. *J. Chem. Phys.* **2024**, *160* (10), No. 107102.

(27) Zhong, Q.; Steinhurst, D. A.; Carpenter, E. E.; Owrutsky, J. C. Fourier Transform Infrared Spectroscopy of Azide Ion in Reverse Micelles. *Langmuir* **2002**, *18* (20), 7401−7408.

(28) Samant, M. G.; Viswanathan, R.; Seki, H.; Bagus, P. S.; Nelin, C. J.; Philpott, M. R. In situ vibrational spectroscopy of specifically adsorbed azide on silver electrodes. *J. Chem. Phys.* **1988**, *89* (1), 583−589.

(29) Dutta, S.; Ren, Z.; Brinzer, T.; Garrett-Roe, S. Two-dimensional ultrafast vibrational spectroscopy of azides in ionic liquids reveals solute-specific solvation. *Phys. Chem. Chem. Phys.* **2015**, *17* (40), 26575−26579.

(30) Tuladhar, A.; Piontek, S. M.; Frazer, L.; Borguet, E. Effect of Halide Anions on the Structure and Dynamics of Water Next to an Alumina (0001) Surface. *J. Phys. Chem. C* **2018**, *122* (24), 12819−12830.

(31) Shiratori, K.; Morita, A. Theory of Quadrupole Contributions from Interface and Bulk in Second-Order Optical Processes. *Bull. Chem. Soc. Jpn.* **2012**, *85* (10), 1061−1076.

(32) Morita, A. *Theory of Sum Frequency Generation Spectroscopy*; Springer, 2018; Vol. *97*.

(33) Mori, W.; Wang, L.; Sato, Y.; Morita, A. Development of quadrupole susceptibility automatic calculator in sum frequency generation spectroscopy and application to methyl C-H vibrations. *J. Chem. Phys.* **2020**, *153* (17), No. 174705.
(34) Andersson, M. P.; Uvdal, P. New scale factors for harmonic vibrational frequencies using the B3LYP density functional method with the triple-zeta basis set 6-311+G(d,p). *J. Phys. Chem. A* **2005**, *109* (12), 2937−2941.
(35) Cramer, C. J. *Essentials of Computational Chemistry: Theories and Models*; Wiley, 2005.
(36) Frisch, M. J.; Trucks, G. W.; Schlegel, H. B.; Scuseria, G. E.; Robb, M. A.; Cheeseman, J. R.; Scalmani, G.; Barone, V.; Petersson, G. A.; Nakatsuji, H.et al. *Gaussian 16 Rev. C.01*, Wallingford, CT, 2016.
(37) Hutter, J.; Iannuzzi, M.; Schiffmann, F.; VandeVondele, J. cp2k: atomistic simulations of condensed matter systems. *WIREs Computational Molecular Sci.* **2014**, *4* (1), 15−25.
(38) VandeVondele, J.; Krack, M.; Mohamed, F.; Parrinello, M.; Chassaing, T.; Hutter, J. Quickstep: Fast and accurate density functional calculations using a mixed Gaussian and plane waves approach. *Comput. Phys. Commun.* **2005**, *167* (2), 103−128.
(39) Perdew, J. P.; Burke, K.; Ernzerhof, M. Generalized Gradient Approximation Made Simple. *Phys. Rev. Lett.* **1996**, *77* (18), 3865−3868.
(40) Perdew, J. P.; Burke, K.; Ernzerhof, M. Generalized Gradient Approximation Made Simple [Phys. Rev. Lett. 77, 3865 (1996)]. *Phys. Rev. Lett.* **1997**, *78* (7), 1396.
(41) Grimme, S.; Antony, J.; Ehrlich, S.; Krieg, H. A consistent and accurate ab initio parametrization of density functional dispersion correction (DFT-D) for the 94 elements H-Pu. *J. Chem. Phys.* **2010**, *132* (15), No. 154104.
(42) Goedecker, S.; Teter, M.; Hutter, J. Separable dual-space Gaussian pseudopotentials. *Phys. Rev. B* **1996**, *54* (3), 1703−1710.
(43) Nosé, S. A unified formulation of the constant temperature molecular dynamics methods. *J. Chem. Phys.* **1984**, *81* (1), 511−519.
(44) Hoover, W. G. Canonical dynamics: Equilibrium phase-space distributions. *Phys. Rev. A* **1985**, *31* (3), 1695−1697.
(45) Verma, P. K.; Kundu, A.; Puretz, M. S.; Dhoonmoon, C.; Chegwidden, O. S.; Londergan, C. H.; Cho, M. The Bend+Libration Combination Band Is an Intrinsic, Collective, and Strongly Solute-Dependent Reporter on the Hydrogen Bonding Network of Liquid Water. *J. Phys. Chem. B* **2018**, *122* (9), 2587−2599.
(46) Liu, H.; Wang, Y.; Bowman, J. M. Quantum Local Monomer IR Spectrum of Liquid D_2O at 300 K from 0 to 4000 cm^{-1} Is in Near-Quantitative Agreement with Experiment. *J. Phys. Chem. B* **2016**, *120* (10), 2824−2828.
(47) Tuladhar, A.; Dewan, S.; Kubicki, J. D.; Borguet, E. Spectroscopy and Ultrafast Vibrational Dynamics of Strongly Hydrogen Bonded OH Species at the α-$Al_2O_3(11\bar{2}0)/H_2O$ Interface. *J. Phys. Chem. C* **2016**, *120* (29), 16153−16161.
(48) Franks, G. V.; Meagher, L. The isoelectric points of sapphire crystals and alpha-alumina powder. *Colloids Surf., A* **2003**, *214*, 99−110.
(49) Stack, A. G.; Higgins, S. R.; Eggleston, C. M. Point of zero charge of a corundum-water interface probed with optical second harmonic generation (SHG) and atomic force microscopy (AFM): New approaches to oxide surface charge. *Geochim. Cosmochim. Acta* **2001**, *65* (18), 3055−3063.
(50) Lützenkirchen, J.; Franks, G. V.; Plaschke, M.; Zimmermann, R.; Heberling, F.; Abdelmonem, A.; Darbha, G. K.; Schild, D.; Filby, A.; Eng, P.; et al. The surface chemistry of sapphire-c: A literature review and a study on various factors influencing its IEP. *Adv. Colloid Interface Sci.* **2018**, *251*, 1−25.
(51) Houchins, C.; Weidinger, D.; Owrutsky, J. C. Vibrational Spectroscopy and Dynamics of the Hydrazoic and Isothiocyanic Acids in Water and Methanol. *J. Phys. Chem. A* **2010**, *114* (24), 6569−6574.
(52) Eyster, E. H.; Gillette, R. H. The Vibration Spectra of Hydrazoic Acid, Methyl Azide, and Methyl Isocyanate The Thermodynamic Functions of Hydrazoic Acid. *J. Chem. Phys.* **1940**, *8* (5), 369−377.
(53) Mollica Nardo, V.; Cassone, G.; Ponterio, R. C.; Saija, F.; Sponer, J.; Tommasini, M.; Trusso, S. Electric-Field-Induced Effects on the Dipole Moment and Vibrational Modes of the Centrosymmetric Indigo Molecule. *J. Phys. Chem. A* **2020**, *124* (51), 10856−10869.
(54) Tadjeddine, A.; Peremans, A.; Guyot-Sionnest, P. Vibrational spectroscopy of the electrochemical interface by visible-infrared sum-frequency generation. *Surf. Sci.* **1995**, *335*, 210−220.
(55) Dadashi, S.; Parshotam, S.; Mandal, B.; Rehl, B.; Gibbs, J. M.; Borguet, E. Influence of Charged Site Density on Local Electric Fields and Polar Solvent Organization at Oxide Interfaces. *J. Phys. Chem. C* **2024**, *128* (23), 9683−9692.
(56) Morita, A.; Kato, S. Vibrational relaxation of azide ion in water: The role of intramolecular charge fluctuation and solvent-induced vibrational coupling. *J. Chem. Phys.* **1998**, *109* (13), 5511−5523.
(57) Harmon, K. J.; Chen, Y.; Bylaska, E. J.; Catalano, J. G.; Bedzyk, M. J.; Weare, J. H.; Fenter, P. Insights on the Alumina−Water Interface Structure by Direct Comparison of Density Functional Simulations with X-ray Reflectivity. *J. Phys. Chem. C* **2018**, *122* (47), 26934−26944.
(58) Shiratori, K.; Morita, A. Molecular theory on dielectric constant at interfaces: A molecular dynamics study of the water/vapor interface. *J. Chem. Phys.* **2011**, *134* (23), No. 234705.

https://doi.org/10.1021/acs.jpcc.4c05318
J. Phys. Chem. C 2024, 128, 21508−21517